Deep-red laser operation of cleaved single-crystal plates of Eu:CsGd(MoO 4) 2 molybdate

Amandine Baillard, Pavel Loiko, Anatoly Pavlyuk, Gurvan Brasse, Alain Braud, Patrice Camy

Deep-red laser operation of cleaved single-crystal plates of Eu:CsGd(MoO$_4$)$_2$ molybdate

AMANDINE BAILLARD,[1] PAVEL LOIKO,[1] ANATOLY PAVLYUK,[2] GURVAN BRASSE,[1] ALAIN BRAUD,[1] AND PATRICE CAMY[1,*]

[1]*Centre de Recherche sur les Ions, les Matériaux et la Photonique (CIMAP), UMR 6252 CEA-CNRS-ENSICAEN, Université de Caen Normandie, 6 Boulevard Maréchal Juin, 14050 Caen Cedex 4, France*
[2]*A.V. Nikolaev Institute of Inorganic Chemistry, Siberian Branch of Russian Academy of Sciences, 3 Lavrentyev Ave., 630090 Novosibirsk, Russia*
**Corresponding author: patrice.camy@ensicaen.fr*

Received XX Month XXXX; revised XX Month, XXXX; accepted XX Month XXXX; posted XX Month XXXX (Doc. ID XXXXX); published XX Month XXXX

We report on the first deep-red laser operation of a heavily Eu^{3+}-doped cesium gadolinium double molybdate crystal with a perfect cleavage. A 17 at.% Eu:CsGd(MoO$_4$)$_2$ laser based on cleaved single-crystal plates generated a maximum continuous-wave output power of 212 mW at 703.1 nm (^{5}D$_0$ → ^{7}F$_4$ transition) with a slope efficiency of 30.1%, a low laser threshold of 51 mW, a linear polarization and a beam quality factor M^2 = 1.6-1.7. This monoclinic crystal is promising for deep-red microchip lasers. © 2023 Optical Society of America

http://dx.doi.org/10.1364/OL.99.099999

Trivalent europium ions (Eu^{3+}) possess an electronic configuration of [Xe]4f^6, with a set of lower-lying ^{7}F$_J$ multiplets (J = 0 - 6, where ^{7}F$_0$ is the ground state), and a metastable state ^{5}D$_0$. They feature red emission of high purity associated with the ^{5}D$_0$ → ^{7}F$_{1,2}$ transitions around 593 and 612 nm, respectively. Owing to this, Eu^{3+} ions are used as red phosphors [1,2] in field emission displays, white LEDs and fluorescent lamps. They are also employed as structural probes to determine the symmetry of crystalline host materials [3,4]. Only a few studies concern the stimulated emission of Eu^{3+} ions in some materials in the red spectral range [5-7].

Deep-red light corresponds to the extreme red end of the visible spectral range at the wavelengths of 660 - 750 nm. It is dimly visible to human eyes but finds multiple applications in biomedicine (e.g., photodynamic / photoimmune therapy, dermatology) as it belongs to photo-biologically active radiation, PBAR, stimulated-emission depletion (STED) microscopy, analytical chemistry, genomics, and matrix-assisted laser desorption and ionization [8,9].

Laser sources directly emitting in the deep-red spectral range can be realized using several rare-earth ions [10], namely, Pr^{3+} [11], Ho^{3+} [12], Er^{3+} [13] and Eu^{3+} [14]. Deep-red emission can also be achieved via frequency conversion of Raman lasers [15]. This spectral range is also covered by Ti:Sapphire lasers. The studies reported to date focused mainly on Pr-lasers operating on the ^{3}P$_0$ → ^{3}F$_3$ and ^{3}F$_4$ transitions around 698 and 717 nm, respectively [16-18]. Xu *et al.* reported on a diode-pumped Pr:LiYF$_4$ laser delivering 348 mW at 697.6 nm with a slope efficiency of 32.7% [18]. Eu^{3+} ions provide deep-red emission according to the ^{5}D$_0$ → ^{7}F$_4$ transition at 703 nm. So far, laser action on this transition was realized using only a few crystals, including Eu:KGd(WO$_4$)$_2$ [19] and Eu:LiYF$_4$ [20]. The first room temperature continuous-wave (CW) laser action was achieved by Dashkevich *et al.* yielding an output power of 5.3 mW at 702.3 nm [19]. Demesh *et al.* reported on a CW Eu:LiYF$_4$ laser generating 15 mW at 701.9 nm with a slope efficiency of 4.6% [20].

The development of deep-red Eu-lasers is constrained by the low absorption cross-sections of Eu^{3+} ions in crystals in the blue-green spectral range (the corresponding transitions are spin-forbidden), together with narrow absorption linewidths (typically below 1 nm). The Eu^{3+} absorption is also not addressed by commercial blue laser diodes. One solution to overcome this problem is to use heavily doped crystals. This is possible as Eu^{3+} ions do not exhibit any cross-relaxation processes affecting the lifetime of the upper laser level (^{5}D$_0$). Recently, Loiko *et al.* used a stoichiometric (100 at.% doped) crystal of KEu(WO$_4$)$_2$ to generate 1.11 W at ~703nm with a slope efficiency of 43.2% and a laser threshold of 64 mW (in the quasi-CW regime) [14]. Another solution is to search for crystals with a strong anisotropy of transition cross-sections.

It is thus relevant to explore other laser host crystals suitable for heavy Eu^{3+} doping featuring a strong anisotropy of spectroscopic properties. Among oxide matrices, one should consequently look at Gd-based ones as the ionic radii of Gd^{3+} and Eu^{3+} are relatively close (1.053 Å and 1.066 Å, respectively, for VIII-fold coordination by O^{2-}). Cesium gadolinium double molybdate, CsGd(MoO$_4$)$_2$, is a promising laser host material [21]. It crystallizes in the monoclinic class (sp. gr. $P2/c$). Rare-earth ions in CsGd(MoO$_4$)$_2$ exhibit a strong anisotropy of absorption and emission cross-sections for polarized light due to a combination of a low rare-earth site symmetry (C$_2$) and a layered crystal structure. It can also accommodate large dopant ions (such as Nd^{3+}) in high concentrations (tens of at.%) [22].

The layered structure of the CsGd(MoO$_4$)$_2$ crystal determines its another interesting feature, namely, a perfect cleavage. It makes it possible to produce crystal plates with a mirror-like surface. Such plates are well suited for the development of microchip lasers (note that CsGd(MoO$_4$)$_2$ crystals exhibit a positive thermal lens) [23,24].

In the present work, we report on the first deep-red laser operation of a heavily Eu^{3+}-doped CsGd(MoO$_4$)$_2$ crystal using crystal plates produced by mechanical cleaving.

Eu:CsGd(MoO$_4$)$_2$ melts incongruently at 1319 K. In the present work, a 17 at.% Eu:CsGd(MoO$_4$)$_2$ crystal was grown from flux under low thermal gradients using cesium trimolybdate (Cs$_2$Mo$_3$O$_{10}$) as a

solvent. The solute/solvent molar ratio was 85-15 mol%. The raw materials were Cs_2CO_3 (purity: 4N), Gd_2O_3, Eu_2O_3 and MoO_3 (5N). The growth was performed in air using a Pt crucible (Φ70 mm, height: 120 mm). First, the crucible was heated slowly to 1298 K and held at this temperature for 20-25 h while constantly stirring to homogenize the solution. Then, the temperature was lowered to the saturation temperature of the solution (1288 K). A seed from an undoped $CsGd(MoO_4)_2$ crystal was oriented along the [100] axis. The rotation speed was 30 rpm, the pulling rate was 0.5-3 mm/day, and the cooling rate was 1-2 K/day. The temperature gradients in the solution were <1 K/cm in the radial direction and <5-10 K/cm in the axial one. After 5-10 days of growth, the crystal was removed from the solution and slowly cooled down to room temperature at a rate of 15 K/h. No post-growth annealing was applied.

The as-grown 17 at % Eu:$CsGd(MoO_4)_2$ boule had a cylindric shape (Φ8-14 mm, length: ~25 mm). The actual Eu^{3+} ion density N_{Eu} determined by Inductively Coupled Plasma atomic spectroscopy was 8.66×10^{20} at/cm^3. The crystal was transparent with a deep rose coloration due to Eu^{3+} doping. Eu:$CsGd(MoO_4)_2$ crystallizes in the monoclinic class (sp. gr. $P2/c$ - C^4_{2h}) and it exhibits a perfect cleavage along the (100) crystallographic plane. This is because the crystal structure is determined by isolated - [Gd|EuO_8] - [MoO_4] – layers in the ***b*-*c*** plane. Crystal plates with flat, smooth and lustrous surfaces were readily produced by mechanical cleaving orthogonal to the growth direction. Under illumination by a UV lamp (362 nm), they exhibited bright red luminescence, Fig. 1(a). Figure 1(b) shows a Scanning Electron Microscope (SEM) image of the lateral boule side showing crystalline layers running parallel to the (100) plane. As revealed by confocal laser microscopy, Fig. 1(c), the cleaved surface is clean, flat and free of defects over a large area up to 1 cm^2. The observation in the interferometric mode indicates a very small root mean square (r.m.s.) surface roughness of a few nm, Fig. 1(d). It originates from kink defects, i.e., steps appearing due to a non-perfect stripping of individual crystalline layers.

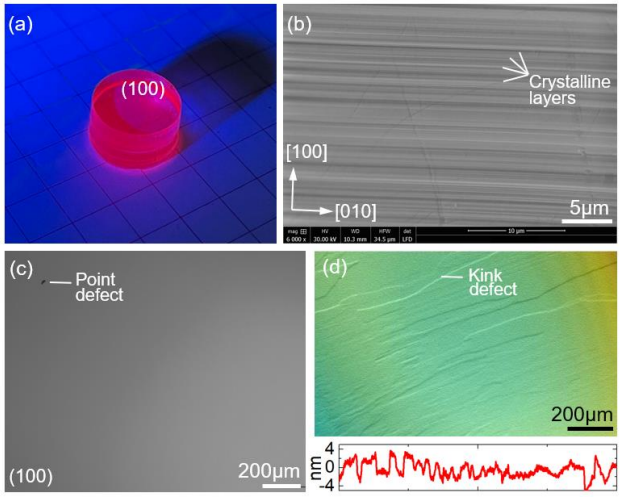

Fig. 1. Cleaving Eu:$CsGd(MoO_4)_2$ crystal: (a) a (100) crystal plate under illumination by a UV lamp (365 nm); (b) a FESEM image of the lateral boule side showing stacked crystalline layers; (c) a (100) cleaved crystal plane observed with a confocal laser microscope; (d) a topography map of this surface and a roughness plot across its diagonal.

A simplified energy-level scheme of Eu^{3+} ions is shown in Fig. 2(a). The pump transition is $^7F_1 \rightarrow {}^5D_1$ falling in the green spectral range. The $^5D_1$ excited-state is short-living ($\tau_{lum} \sim 8$ μs) as it is depopulated by the multiphonon non-radiative (NR) relaxation. The terminal laser manifold ($^7F_4$) for the deep-red laser transition, $^5D_0 \rightarrow {}^7F_4$, is also drained via the NR path. Thus, this transition represents a four-level laser scheme.

We briefly characterized the key spectroscopic properties of Eu^{3+} ions in the $CsGd(MoO_4)_2$ crystal relevant for laser experiments. For the $^7F_1 \rightarrow {}^5D_1$ transition falling in the green, the peak absorption cross-section σ_{abs} is 0.70×10^{-20} cm^2 at 534.7 nm while the absorption bandwidth (full width at half maximum) is only 1.0 nm (for light polarization ***E*** || ***b***), Fig. 2(b). For other two polarizations, the absorption is by an order of magnitude weaker highlighting the need of polarized pumping.

The stimulated-emission (SE) cross-sections, σ_{SE}, were calculated via the Füchtbauer–Ladenburg formula [25] using the radiative lifetime of the $^5D_0$ state (τ_{rad} = 0.89 ms) and the luminescence branching ratios for the $^5D_0 \rightarrow {}^7F_J$ transitions (β_{02} = 71.1% and β_{04} = 19.2%) obtained using the Judd-Ofelt theory. The corresponding intensity parameters were $\Omega_2 = 10.91$, $\Omega_4 = 6.06$ and $\Omega_6 = 1.55$ [10^{-20} cm^2]. The emission spectra are strongly polarized, Fig. 2(c). The peak σ_{SE} is 11.5×10^{-20} cm^2 at 614.2 nm ($^5D_0 \rightarrow {}^7F_2$, red emission) and 1.81×10^{-20} cm^2 at 703.3 nm ($^5D_0 \rightarrow {}^7F_4$, deep-red one) for polarization ***E*** || ***b***. The luminescence decay curve from the $^5D_0$ Eu^{3+} state measured under ns pulse excitation is single-exponential and the corresponding lifetime τ_{lum} is 692 μs. Eu^{3+} ions in $CsGd(MoO_4)_2$ replace for the Gd^{3+} cations in a single type of sites (C_2 symmetry, VIII-fold coordination).

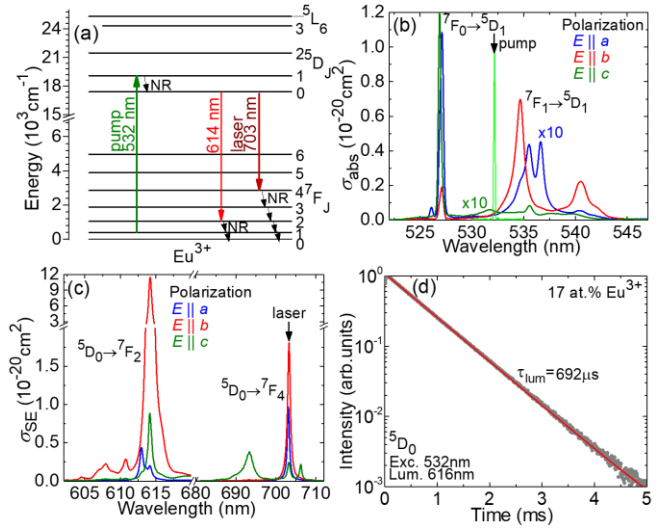

Fig. 2. (a) The energy-level diagram of Eu^{3+} ions; (b-d) Spectroscopy of Eu^{3+} ions in the 17 at.% Eu:$CsGd(MoO_4)_2$ crystal: (b) absorption cross-sections, σ_{abs}, the $^7F_{0,1} \rightarrow {}^5D_1$ transition; (c) SE cross-sections, σ_{SE}, the $^5D_0 \rightarrow {}^7F_2$ and $^7F_4$ transitions; (d) luminescence decay curve. *Arrows* in (b,d) indicate the pump and laser wavelengths.

The laser set-up is depicted in Fig. 3(a). The laser element was fabricated by mechanical cleaving along the (100) plane of an as-grown 17 at.% Eu:$CsGd(MoO_4)_2$ crystal. It was oriented for light propagation along the ***a***-axis. It had a cylindric shape (diameter / clear aperture: 9 mm, thickness: 5.0 mm). No polishing was applied to the cleaved input and output faces. The sample was mounted on

a Cu-holder without active cooling and a silver paint was used for better heat removal. A plano-plano cavity was formed by a pump mirror (PM) coated for high transmission (HT, T = 85%) at 0.53 μm and high reflection (HR, R > 99.96%) at 0.59 – 0.72 μm, and a set of output couplers (OCs) with a transmission at the laser wavelength (0.70 μm) T_{OC} in the range of 0.02% - 2.39%. Both cavity mirrors were placed close to the crystal faces with airgaps less than 1 mm, so that the geometrical cavity length was 6 mm, see the photograph in Fig. 3(b). The pump source was a commercial solid-state laser (Millennia Prime, Spectra Physics) emitting up to 10 W at 532.2 nm (laser linewidth: 0.15 nm) with a diffraction limited beam ($M^2 \approx 1$) and a linear polarization. It addressed the $^7F_1 \rightarrow {}^5D_1$ transition of Eu^{3+} ions. The polarization of the pump radiation was adjusted by an AR-coated half-wave wave plate, and it corresponded to $\boldsymbol{E}_P \parallel \boldsymbol{b}$ in the crystal. The pump beam was focused into the crystal through the PM using an AR-coated achromatic lens (f = 75 mm) resulting in a pump spot radius of 40±5 μm. The incident pump power was limited to 3.2 W to avoid the crystal fracture. The pumping was in single pass. The pump absorption was weakly dependent on the pump level and amounted to 24.8% (including the Fresnel loss at the uncoated input facet), Fig. 3(c). The residual pump after the OC was filtered out using a long-pass filter (LP600, Thorlabs). The spectra were measured using an optical spectrum analyzer (Ando AQ6315E) and the beam profile in the far-field was captured using a CCD-camera (Bladecam-XHR, Dataray). The M^2 factor was measured by an ISO-standard technique using a focusing lens (f = 100 mm) for creating a secondary beam waist.

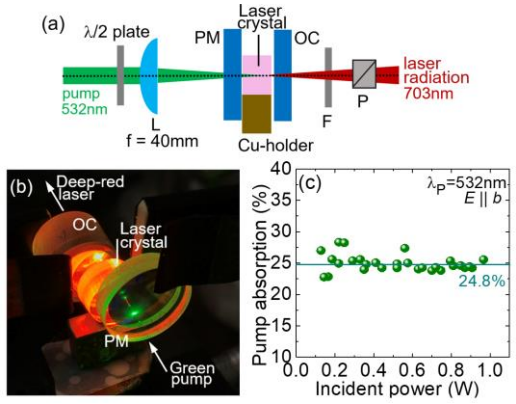

Fig. 3. $Eu:CsGd(MoO_4)_2$ laser: (a) layout of the laser set-up, L – AR-coated achromatic lens, PM – pump mirror, OC – output coupler, F – cut-off filter, P – Glan-Taylor polarizer; (b) a photo of the laser; (c) measured single-pass pump absorption.

The $Eu:CsGd(MoO_4)_2$ laser generated a maximum output power of 212 mW at 703.1 nm (laser linewidth: <0.1 nm) with a slope efficiency η of 30.1% (vs. the absorbed pump power) and a low laser threshold of 51 mW (for T_{OC} = 0.25%), Fig. 4(a). This corresponded to an incident pump power of 3.17 W, so that the optical efficiency of 6.7% (this low value was mainly due to the relatively weak pump absorption in the laser crystal). For higher output coupling, the laser threshold increased from 19 mW (for T_{OC} = 0.02%) to 98 mW (for T_{OC} = 2.39%). The observed low-threshold behavior is due to the quasi-four-level laser scheme of the $^5D_0 \rightarrow {}^7F_4$ Eu^{3+} transition with no reabsorption. With increasing the output coupling (T_{OC} > 1%), a thermal roll-over was observed in the input-output dependences for the incident pump powers above 2 W. The laser operation in the plano-plano cavity indicates a positive thermal lens of the crystal.

The spectra of laser emission are shown in Fig. 4(b). The Eu-laser operated solely on the $^5D_0 \rightarrow {}^7F_4$ transition (in the deep-red). The laser wavelength (~703 nm) was weakly dependent on the output coupling. Note that the cavity mirrors also supported oscillations in the red spectral range. For some output couplers, we observed what we believe to be amplified spontaneous emission (ASE) at ~614 nm corresponding to the $^5D_0 \rightarrow {}^7F_2$ transition. The reasons for the lack of laser operation on this transition in Eu^{3+}-doped crystals at room temperature are not yet clear. The two possible reasons are the resonant excited-state absorption from the metastable $^5D_0$ Eu^{3+} manifold or reabsorption from the thermally populated terminal laser level ($^7F_2$). Chang employed cryogenic cooling to the liquid N_2 temperature to achieve lasing in a 5 at.% $Eu:Y_2O_3$ crystal [26], however, as broadband silver coated cavity mirrors were used, it is not clear which laser transition was involved.

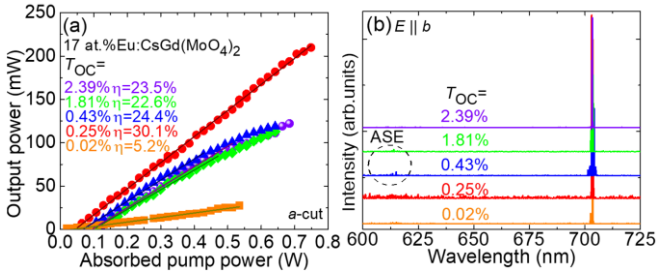

Fig. 4. Deep-red $Eu:CsGd(MoO_4)_2$ laser based on a cleaved crystal plate (***a***-cut): (a) input-output dependences, η – slope efficiency; (b) typical spectra of laser emission, laser polarization: $\boldsymbol{E} \parallel \boldsymbol{b}$.

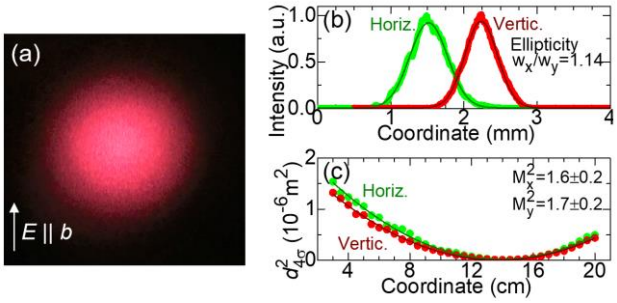

Fig. 5. Spatial characteristics of deep-red emission (~703 nm) from the $Eu:CsGd(MoO_4)_2$ laser: (a) a photograph of a laser beam on a black screen in the far-field; (b) 1D intensity profiles (*symbols* – experimental data, *curves* – Gaussian fits); (c) evaluation of $M^2_{x,y}$ parameters.

A photograph of the deep-red laser beam on a black screen in the far-field is shown in Fig. 5(a). The 1D intensity profiles along the horizonal (x) and vertical (y) directions are shown in Fig. 5(b). They are reasonably well fitted with a Gaussian profile. A slight beam ellipticity of w_x/w_y = 1.14 is detected and ascribed to the astigmatic thermal lens of the laser crystal. The beam quality factors of the laser mode were measured at the maximum output power by an ISO standard procedure, see Fig. 5(c), and amounted to $M^2_{x,y}$ = 1.6-1.7±0.2 indicating a fundamental transverse mode operation with a small admixture of higher-order modes. Their generation is favored

by the four-level laser scheme of Eu^{3+}.

The emission of the deep-red Eu-laser was linearly polarized. The polarization state ($\boldsymbol{E} \parallel \boldsymbol{b}$) was naturally selected by the anisotropy of the gain, Fig. 2(c). The polarization state was characterized using a Glan-Taylor placed after the OC, see Fig. 6. The experimental points were well fitted using a formula $P(\theta) = P_u/2 + P_p\cos^2(\theta - 90°)$, where P_u and P_p are the unpolarized and polarized power fractions and θ is the angle between the polarizer (P) axis and the *x*-axis. The polarization degree $X = P_p/(P_p + P_u)$ was close to unity.

We also adjusted the pump polarization ($\boldsymbol{E}_P$) using the λ/2 plate: the maximum output power of the deep-red laser corresponded to $\boldsymbol{E}_P \parallel \boldsymbol{b}$ and no lasing was observed when pumping into the $\boldsymbol{E}_P \parallel \boldsymbol{c}$ in agreement with the anisotropy of absorption cross-sections for the $^7F_1 \rightarrow {}^5D_1$ transition, Fig. 2(b).

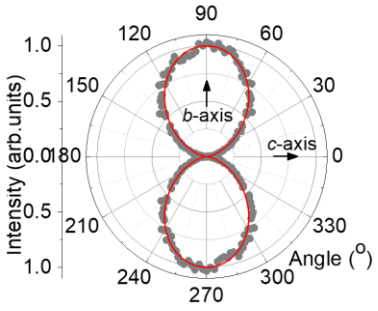

Fig. 6. Analysis of polarization state of laser emission from the deep-red Eu:$CsGd(MoO_4)_2$ laser, T_{OC} = 0.25%, P_{abs} = 0.58 W.

The developed laser represents the first exploitation of the cleavage feature for the $CsGd(MoO_4)_2$ molybdate thus entering the family of cleaving laser crystals which are not numerous, these including borates (LaB_3O_6) [27], phosphates (YPO_4, $LuPO_4$) [28] and molybdates ($KY(MoO_4)_2$, $BaGd_2(MoO_4)_4$) [29,30].

To conclude, the Eu^{3+}-doped $CsGd(MoO_4)_2$ crystal appears as an attractive gain medium for compact low-threshold lasers directly emitting in the deep-red spectral range according to the $^5D_0 \rightarrow {}^7F_4$ transition because of a combination of appealing properties: (i) high available doping levels (tens of at.% Eu^{3+}) and a weak luminescence quenching, (ii) high absorption / emission cross-sections for polarized light, (iii) relatively long upper laser level lifetime, (iv) perfect cleavage feature and (v) positive thermal lensing allowing for the microchip operation. It also benefits from a relatively low melting point. We report on the first laser action in this compound in the deep-red spectral range in the CW regime. We also observed the signatures of amplified spontaneous emission for the red laser transition, $^5D_0 \rightarrow {}^7F_2$, at 614 nm which require further investigations.

Funding. Agence Nationale de la Recherche (ANR-22-CE08-0025-01, NOVELA); Fonds européen de développement régional (FEDER); Contrat de plan État-Région(CPER) de Normandie.

Disclosures. The authors declare no conflicts of interest.

Data availability. Data underlying the results presented in this paper are not publicly available at this time but may be obtained from the authors upon reasonable request.

References

1. J. Li, J. Yan, D. Wen, W. U. Khan, J. Shi, M. Wu, Q. Su, and P. A. Tanner, J. Mater. Chem. C **4**, 8611 (2016).
2. M. M. Haque, H. I. Lee, and D. K. Kim, J. Alloys Compd. **481**, 792 (2009).
3. G. Jia, P. A. Tanner, C. K. Duan, and J. Dexpert-Ghys, J. Phys. Chem. C **114**, 2769 (2010).
4. A. Volokitina, P. Loiko, E. Vilejshikova, X. Mateos, E. Dunina, A. Kornienko, N. Kuleshov, and A. Pavlyuk, J. Alloys Compd. **762**, 786 (2018).
5. J. H. Park and A. J. Steckl, Appl. Phys. Lett. **85**, 4588 (2004).
6. K. Nakamura, Y. Hasegawa, H. Kawai, N. Yasuda, N. Kanehisa, Y. Kai, T. Nagamura, S. Yanagida, and Y. Wada, J. Phys. Chem. A **111**, 3029 (2007).
7. P. A. Loiko, V. I. Dashkevich, S. N. Bagaev, V. A. Orlovich, A. S. Yasukevich, K. V. Yumashev, N. V. Kuleshov, E. B. Dunina, A. A. Kornienko, S. M. Vatnik, and A. A. Pavlyuk, Laser Phys. **23**, 105811 (2013).
8. J. B. Ding, K. T. Takasaki, and B. L. Sabatini, Neuron **63**, 429 (2009).
9. M. Alexiades-Armenakas, Clin. Dermatol. **24**, 16 (2006).
10. C. Kränkel, D.-T. Marzahl, F. Moglia, G. Huber, and P. W. Metz, Laser Photon. Rev. **10**, 548 (2016).
11. Z. Liu, Z. Cai, S. Huang, C. Zeng, Z. Meng, Y. Bu, Z. Luo, B. Xu, H. Xu, C. Ye, F. Stareki, P. Camy, and R. Moncorgé, J. Opt. Soc. Am. B **30**, 302 (2013).
12. S. Ji, S. Huang, Z. Wang, X. Lin, B. Xiao, H. Xu, and Z. Cai, J. Light. Technol. **41**, 301 (2023).
13. M. Knights, W. Wing, J. Baer, E. Chicklis, and H. Jenssen, IEEE J. Quantum Electron. **18**, 163 (1982).
14. P. Loiko, D. Rytz, S. Schwung, P. Pues, T. Jüstel, J.-L. Doualan, and P. Camy, Opt. Lett. **46**, 2702 (2021).
15. H. Zhao, C.-H. Lin, C. Jiang, S.-B. Dai, H.-Q. Zhou, S.-Q. Zhu, H. Yin, Z. Li, and Z.-Q. Chen, Opt. Express **31**, 265 (2023).
16. W. Li, T. Du, J. Lan, C. Guo, Y. Cheng, H. Xu, C. Zhu, F. Wang, Z. Luo, and Z. Cai, Opt. Lett. **42**, 671 (2017).
17. S. Luo, X. Yan, Q. Cui, B. Xu, H. Xu, and Z. Cai, Opt. Commun. **380**, 357 (2016).
18. B. Xu, Y. Cheng, B. Qu, S. Luo, H. Xu, Z. Cai, P. Camy, J.-L. Doualan, and R. Moncorgé, Opt. Laser Technol. **67**, 146 (2015).
19. V. I. Dashkevich, S. N. Bagayev, V. A. Orlovich, A. A. Bui, P. A. Loiko, K. V. Yumashev, N. V. Kuleshov, S. M. Vatnik, and A. A. Pavlyuk, Laser Phys. Lett. **12**, 015006 (2015).
20. M. Demesh, A. Yasukevich, V. Kisel, E. Dunina, A. Kornienko, V. Dashkevich, V. Orlovich, E. Castellano-Hernández, C. Kränkel, and N. Kuleshov, Opt. Lett. **43**, 2364 (2018).
21. P. Loiko, A. Pavlyuk, S. Slimi, R. M. Sole, E. B. Salem, E. Dunina, A. Kornienko, P. Camy, U. Griebner, V. Petrov, F. Díaz, M. Aguilo, and X. Mateos, J. Lumin. **231**, 117793 (2021).
22. A. A. Pavlyuk, L. I. Kozeeva, K. G. Folin, V. G. Gladyshev, V. S. Gulyaev, V. S. Pivtsov, and A. A. Kaminskii, Inorg. Mater. **19**, 767 (1983).
23. A. Volokitina, P. Loiko, A. Pavlyuk, S. Slimi, R. M. Solé, E. B. Salem, E. Kifle, J. M. Serres, U. Griebner, V. Petrov, M. Aguiló, F. Díaz, and X. Mateos, Opt. Express **28**, 9039 (2020).
24. W. Zhao, Y.-S. Huang, Z.-B. Lin, B. Wei, F.-W. Wang, M. Xu, X. Zhao, Q.-H. Zheng, and W.-W. Zhou, RSC Adv. **5**, 34730 (2015).
25. B. Aull, H. Jenssen, IEEE J. Quantum Electron. **18**, 925 (1982).
26. N. C. Chang, J. Appl. Phys. **34**, 3500 (1963).
27. Y. Chen, X. Gong, Y. Lin, Q. Tan, Z. Luo, and Y. Huang, Appl. Opt. **45**, 8338 (2006).
28. J. Liu, W. Han, X. Chen, D. Zhong, B. Teng, C. Wang, and Y. Li, Opt. Lett. **39**, 5881 (2014).
29. Y. J. Chen, Y. F. Lin, X. H. Gong, H. M. Zhu, Z. D. Luo, and Y. D. Huang, Appl. Phys. B **98**, 55 (2010).
30. A. Volokitina, P. Loiko, A. Pavlyuk, J. M. Serres, S. Slimi, E. B. Salem, E. Kifle, U. Griebner, V. Petrov, L. Wang, W. Chen, R. M. Solé, M. Aguiló, F. Díaz, and X. Mateos, Opt. Mater. Express **10**, 2356 (2020).

Full references

1. J. Li, J. Yan, D. Wen, W. U. Khan, J. Shi, M. Wu, Q. Su, and P. A. Tanner, "Advanced red phosphors for white light-emitting diodes," J. Mater. Chem. C **4**(37), 8611-8623 (2016).
2. M. M. Haque, H. I. Lee, and D. K. Kim, "Luminescent properties of Eu^{3+}-activated molybdate-based novel red-emitting phosphors for LEDs," J. Alloys Compd. **481**(1-2), 792-796 (2009).
3. G. Jia, P. A. Tanner, C. K. Duan, and J. Dexpert-Ghys, "Eu^{3+} spectroscopy: a structural probe for yttrium orthoborate phosphors," J. Phys. Chem. C **114**(6), 2769-2775 (2010).
4. A. Volokitina, P. Loiko, E. Vilejshikova, X. Mateos, E. Dunina, A. Kornienko, N. Kuleshov, and A. Pavlyuk, "Eu^{3+}:$KY(MoO_4)_2$: A novel anisotropic red-emitting material with a layered structure," J. Alloys Compd. **762**, 786-796 (2018).
5. J. H. Park and A. J. Steckl, "Laser action in Eu-doped GaN thin-film cavity at room temperature," Appl. Phys. Lett. **85**, 4588-4590 (2004).
6. K. Nakamura, Y. Hasegawa, H. Kawai, N. Yasuda, N. Kanehisa, Y. Kai, T. Nagamura, S. Yanagida, and Y. Wada, "Enhanced lasing properties of dissymmetric Eu(III) complex with bidentate phosphine ligands," J. Phys. Chem. A **111**(16), 3029-3037 (2007).
7. P. A. Loiko, V. I. Dashkevich, S. N. Bagaev, V. A. Orlovich, A. S. Yasukevich, K. V. Yumashev, N. V. Kuleshov, E. B. Dunina, A. A. Kornienko, S. M. Vatnik, and A. A. Pavlyuk, "Spectroscopic characterization and pulsed laser operation of Eu^{3+}:$KGd(WO_4)_2$ crystal," Laser Phys. **23**, 105811 (2013).
8. J. B. Ding, K. T. Takasaki, and B. L. Sabatini, "Supraresolution imaging in brain slices using stimulated-emission depletion two-photon laser scanning microscopy," Neuron **63**(4), 429-437 (2009).
9. M. Alexiades-Armenakas, "Laser-mediated photodynamic therapy," Clin. Dermatol. **24**(1), 16-25 (2006).
10. C. Kränkel, D.-T. Marzahl, F. Moglia, G. Huber, and P. W. Metz, "Out of the blue: semiconductor laser pumped visible rare-earth doped lasers," Laser Photon. Rev. **10**(4), 548-568 (2016).
11. Z. Liu, Z. Cai, S. Huang, C. Zeng, Z. Meng, Y. Bu, Z. Luo, B. Xu, H. Xu, C. Ye, F. Stareki, P. Camy, and R. Moncorgé, "Diode-pumped Pr^{3+}:$LiYF_4$ continuous-wave deep red laser at 698 nm," J. Opt. Soc. Am. B **30**, 302-305 (2013).
12. S. Ji, S. Huang, Z. Wang, X. Lin, B. Xiao, H. Xu, and Z. Cai, "Watt-level high-efficiency deep-red Ho^{3+}:ZBLAN fiber laser," J. Light. Technol. **41**(1), 301-306 (2023).
13. M. Knights, W. Wing, J. Baer, E. Chicklis, and H. Jenssen, "High-efficiency deep-red laser pumped by doubled Nd:YAG," IEEE J. Quantum Electron. **18**(2), 163-166 (1982).
14. P. Loiko, D. Rytz, S. Schwung, P. Pues, T. Jüstel, J.-L. Doualan, and P. Camy, "Watt-level europium laser at 703 nm", Opt. Lett. **46**, 2702-2705 (2021).
15. H. Zhao, C.-H. Lin, C. Jiang, S.-B. Dai, H.-Q. Zhou, S.-Q. Zhu, H. Yin, Z. Li, and Z.-Q. Chen, "Wavelength-versatile deep-red laser source by intracavity frequency converted Raman laser," Opt. Express **31**, 265-273 (2023).
16. W. Li, T. Du, J. Lan, C. Guo, Y. Cheng, H. Xu, C. Zhu, F. Wang, Z. Luo, and Z. Cai, "716 nm deep-red passively Q-switched Pr:ZBLAN all-fiber laser using a carbon-nanotube saturable absorber," Opt. Lett. **42**, 671-674 (2017).
17. S. Luo, X. Yan, Q. Cui, B. Xu, H. Xu, and Z. Cai, "Power scaling of blue-diode-pumped Pr:YLF lasers at 523.0, 604.1, 606.9, 639.4, 697.8 and 720.9nm," Opt. Commun. **380**, 357-360 (2016).
18. B. Xu, Y. Cheng, B. Qu, S. Luo, H. Xu, Z. Cai, P. Camy, J.-L. Doualan, and R. Moncorgé, "InGaN-LD-pumped Pr^{3+}:$LiYF_4$ continuous-wave deep red lasers at 697.6 and 695.8nm," Opt. Laser Technol. **67**, 146-149 (2015).
19. V. I. Dashkevich, S. N. Bagayev, V. A. Orlovich, A. A. Bui, P. A. Loiko, K. V. Yumashev, N. V. Kuleshov, S. M. Vatnik, and A. A. Pavlyuk, "Quasi-CW and CW laser operation of Eu:$KGd(WO_4)_2$ crystal on $^5D_0 \rightarrow {}^7F_4$ transition," Laser Phys. Lett. **12**(1), 015006 (2015).
20. M. Demesh, A. Yasukevich, V. Kisel, E. Dunina, A. Kornienko, V. Dashkevich, V. Orlovich, E. Castellano-Hernández, C. Kränkel, and N. Kuleshov, "Spectroscopic properties and continuous-wave deep-red laser operation of Eu^{3+}-doped $LiYF_4$", Opt. Lett. **43**(10), 2364-2367 (2018).
21. P. Loiko, A. Pavlyuk, S. Slimi, R. M. Sole, E. B. Salem, E. Dunina, A. Kornienko, P. Camy, U. Griebner, V. Petrov, F. Díaz, M. Aguilo, and X. Mateos, "Growth, spectroscopy and laser operation of monoclinic Nd:$CsGd(MoO_4)_2$ crystal with a layered structure," J. Lumin. **231**, 117793 (2021).
22. A. A. Pavlyuk, L. I. Kozeeva, K. G. Folin, V. G. Gladyshev, V. S. Gulyaev, V. S. Pivtsov, and A. A. Kaminskii, "Stimulated-emission of the transition $^4F_{3/2} \rightarrow {}^4I_{11/2}$ of Nd^{3+} ions in $RbNd(MoO_4)_2$ and $CsNd(MoO_4)_2$," Inorg. Mater. **19**, 767-768 (1983).
23. A. Volokitina, P. Loiko, A. Pavlyuk, S. Slimi, R. M. Solé, E. B. Salem, E. Kifle, J. M. Serres, U. Griebner, V. Petrov, M. Aguiló, F. Díaz, and X. Mateos, "Laser operation of cleaved single-crystal plates and films of Tm:$KY(MoO_4)_2$," Opt. Express **28**(7), 9039-9048 (2020).
24. W. Zhao, Y.-S. Huang, Z.-B. Lin, B. Wei, F.-W. Wang, M. Xu, X. Zhao, Q.-H. Zheng, and W.-W. Zhou, "Spectra and energy levels of a layered Yb^{3+}:$CsGd(MoO_4)_2$ crystal with perfect cleavage: a candidate for microchip laser," RSC Adv. **5**, 34730-34736 (2015).
25. B. Aull, H. Jenssen, "Vibronic interactions in Nd:YAG resulting in nonreciprocity of absorption and stimulated emission cross sections," IEEE J. Quantum Electron. **18**, 925-930 (1982).
26. N. C. Chang, "Fluorescence and stimulated emission from trivalent europium in yttrium oxide," J. Appl. Phys. **34**(12), 3500-3504 (1963).
27. Y. Chen, X. Gong, Y. Lin, Q. Tan, Z. Luo, and Y. Huang, "Continuous-wave laser characteristics of a Nd^{3+}:LaB_3O_6 cleavage microchip and the influence of thermal effects," Appl. Opt. **45**(32), 8338–8345 (2006)
28. J. Liu, W. Han, X. Chen, D. Zhong, B. Teng, C. Wang, and Y. Li, "Spectroscopic properties and continuous-wave laser operation of Yb:$LuPO_4$ crystal," Opt. Lett. **39**(20), 5881–5884 (2014).
29. Y. J. Chen, Y. F. Lin, X. H. Gong, H. M. Zhu, Z. D. Luo, and Y. D. Huang, "805-nm diode-pumped continuous-wave 2-μm laser performance of Tm^{3+}:$BaGd_2(MoO_4)_4$ cleavage plate," Appl. Phys. B **98**(1), 55-60 (2010).
30. A. Volokitina, P. Loiko, A. Pavlyuk, J. M. Serres, S. Slimi, E. B. Salem, E. Kifle, U. Griebner, V. Petrov, L. Wang, W. Chen, R. M. Solé, M. Aguiló, F. Díaz, and X. Mateos, "Spectroscopy and efficient laser operation of cleaving Yb:$KY(MoO_4)_2$ crystal," Opt. Mater. Express **10**(10), 2356-2369 (2020).